Journal of Polymer Science

WILEY

JOURNAL OF POLYMER SCIENCE

RESEARCH ARTICLE OPEN ACCESS

Multi-Responsive Nanogels Based on Sulfoxide Polymethacrylates for Biomedical Applications

Hannah Elodie Stauber[1] | Clara López-Iglesias[1,2] | Sidra Kanwal[1] | Elisa Quaas[3] | Daniel Klinger[1]

[1]Institute of Pharmacy (Pharmaceutical Chemistry), Freie Universität Berlin, Berlin, Germany | [2]Department of Pharmacology, Pharmacy and Pharmaceutical Technology, I+D Farma Group (GI-1645), Faculty of Pharmacy, Instituto de Materiales (iMATUS) and Health Research Institute of Santiago de Compostela (IDIS), Universidade de Santiago de Compostela, Santiago de Compostela, Spain | [3]Institute of Chemistry and Biochemistry, Freie Universität Berlin, Berlin, Germany

Correspondence: Daniel Klinger (daniel.klinger@fu-berlin.de)

Received: 16 December 2024 | **Revised:** 21 January 2025 | **Accepted:** 30 January 2025

Funding: C.L.-I. acknowledges Xunta de Galicia (Consellería de Cultura, Educación e Ordenación Universitaria) for a postdoctoral fellowship [ED481B-2021-008]. Sidra Kanwal acknowledges the German Academic Exchange Program (DAAD) for the scholarship granted for her PhD studies [57507871].

Keywords: drug delivery | low fouling | nanogels | polysulfoxides | thermo-responsiveness

ABSTRACT

Nanogels for biomedical applications require polymeric building blocks that show high hydrophilicity and (thermo-)responsive properties without immune response risks. Polysulfoxides offer these advantages but have not yet been translated to 3-dimensional colloidal materials. To examine their potential as alternatives to established systems, we developed a synthetic platform with synthetic control and chemical versatility. For this, we utilize the thermo-responsive properties of a polymethacrylate with propyl sulfoxide side groups, that is, poly(2-(*n*-propyl-sulfoxide)ethyl methacrylate) (P(*n*Pr-SEMA)). Its phase transition near body temperature enables nanogel preparation via conventional precipitation polymerization in an all-aqueous system. To fully assess this approach's potential, we first demonstrate control over colloidal properties like size, size distribution, and crosslinking density. We examine the influence of these parameters on the temperature-dependent swelling profiles and develop a standard synthetic protocol. Second, we examine synthetic versatility to introduce additional stimuli-responsiveness. For this, we introduce methacrylic acid (MAA) as pH-responsive co-monomer and examine resulting double-sensitive swelling. Third, we add network degradability through reduction-cleavable crosslinker bis(2-methacryloyloxyethyl) disulfide (DSDMA). Fourth, we demonstrate that multi-responsive nanogels exhibit low cytotoxicity and high colloidal stability in biologically relevant media. Overall, this systematic study establishes P(*n*Pr-SEMA)-based nanogels as versatile alternatives to established temperature-responsive nanogels for biomedical applications, for example, drug delivery.

1 | Introduction

Nanogels (NGs) are soft colloidal particles that contain a crosslinked polymer network. The combination of small size, swollen structure, and colloidal stability renders them interesting materials for applications like drug delivery [1], photonic crystals [2], and (bio-)catalysis [3]. For biomedical applications, their properties need to be controlled with high accuracy. This can be achieved through two features: (a) the internal network structure and (b) the external surface.

Abbreviations: APS, ammonium persulfate; DGS, degree of swelling; DLS, dynamic light scattering; DSDMA, bis(2-methacryloyloxyethyl) disulfide; DTT, dithiothreitol; LC, loading capacity; LCST, lower critical solution temperature; MAA, methacrylic acid; *n*Pr-SEMA, P(*n*Pr-SEMA); NTA, nanoparticle tracking analysis; PBS, phosphate buffered saline; PEG, poly ethylene glycol; SDS, sodium dodecyl sulfate; Tcp, cloud point temperature; TEGDMA, tetraethylene glycol dimethacrylate; TEM, transmission electron microscopy; Vcollapsed, particle volume in the collapsed state; VPTT, volume phase transition temperature; Vswollen, particle volume in the swollen state.

Regarding the internal network, the chemistry of the polymeric building blocks governs stimuli-responsiveness [4, 5], amphiphilicity [6, 7], diffusional properties [8], and (bio-)degradability [5, 9]. Among these characteristics, stimuli-responsiveness is particularly advantageous for biomedical applications, as it allows materials to adapt dynamically to physiological conditions such as changes in pH [10], enzymatic activity [11], or temperature [12]. Thermo-responsive behavior might be of interest to deliver therapeutic agents as passive response to an increased skin [13] or body temperature [14]. Alternatively, delivery can also be triggered actively by photothermal effects in combinations of thermo-responsive NGs and gold nanoparticles [15].

Regarding the external surface, dangling chains of the network control the NGs' interaction with the surrounding aqueous medium and biological (macro-)molecules. For example, an unwanted adsorption of plasma proteins can limit the NGs' biocompatibility, that is, colloidal stability [16], blood circulation time [17], cellular uptake [18], cytotoxicity [19], and biodistribution [20–22]. To reduce such non-specific interactions and provide stimuli-responsiveness, oligoethylene glycol-based methacrylates (OEGMAs) are often used to combine the highly hydrophilic character of polyethylene glycol (PEG) [23, 24] with a thermo-responsive swelling behavior [25]. While OEGMA monomers can easily be copolymerized with functional co-monomers and crosslinkers to incorporate additional responsive properties [26], an inherent drawback of poly-/oligoethylene glycol-based materials is their potential immunogenic effect upon long-term exposure [24, 27, 28]. Alternatively, microgels based on P(NIPAm) are of great interest due to their thermo-responsive swelling behavior close to human body temperature (VPTT; usually around 32°C [29, 30]), however, they are inferior in terms of biocompatibility and biodegradability compared to PEG-based materials [25].

Nevertheless, there is no "one-fits-all" system: Since all monomers differ in their chemical structure, specific applications require specific monomers to precisely adjust the interaction of the polymer network with embedded compounds or external biological systems. Thus, generally, new alternative polymers are needed that do not yet trigger any immune responses, show well-defined thermo-responsive behavior, and are easily accessible from a synthetic perspective.

Polysulfoxides may fulfill these requirements. Especially poly(meth)acrylates and poly(meth)acrylamides with polar methyl sulfoxide side groups are re-emerging as highly hydrophilic polymers that can incorporate functional co-monomers [31–33]. The unique highly dipolar nature of the sulfoxide side groups (similar to DMSO) favors their interaction with biomolecules, favoring their penetration through biological membranes and stabilization of proteins through hydrogen bonding [34]. The corresponding low cytotoxicity has made them potential alternatives to PEG in drug delivery [35], molecular imaging [36], and cryoprotection applications [37]. The outstanding hydrophilic character of methyl sulfoxide-based polymers has been used to impart antifouling properties in 2D materials, such as in surface-bound polymer brushes or polymer coatings [31, 38, 39].

To introduce additional thermo-responsiveness into this class of materials, we have recently shown that introducing hydrophobic alkyl chains on the sulfoxide group can impart cloud point temperature close to body temperature [34]. In these polymers, strong H-bonds favor solubilization of the sulfoxide moieties at lower temperatures. At higher temperatures, dispersive hydrophobic forces between the alkyl groups cause phase separation of the polymer chains. We have shown that the corresponding cloud point temperature (T_{CP}) can be tuned precisely by the structure of the pendant alkyl group. As a result, we have identified poly(2-(*n*-propyl-sulfoxide)ethyl methacrylate) (P(*n*Pr-SEMA)) as a polymer with a phase transition near body temperature, that is, T_{CP} = 30°C–40°C (depending on molecular weight, concentration, and ionic strength). Consequently, these polymers represent interesting potential alternatives to conventional polymeric building blocks for thermo-responsive nano−/microgels like P(OEGMA), P(NIPAm), and so forth.

However, translating such properties into (stimuli-responsive) 3D NGs has not yet been described. A respective synthetic platform should allow controlling two main features: First, it should be possible to adjust the chemical network composition by combining the sulfoxide monomers with functional co-monomers and crosslinkers. Second, the approach should afford control over colloidal properties such as NG size and size distribution. Third, the method should circumvent the use of organic solvents.

To address this need, we exploit the thermo-responsive properties of our polysulfoxide building blocks for their utilization in precipitation polymerizations. Key to this approach is the reduction of polymer solubility upon heating. For such polymers, free radical polymerization in aqueous solution should proceed until growing oligomers reach a critical length where reaction temperature triggers their precipitation into NG nuclei that grow into nanogels upon polymerization [40]. Thus, the thermo-responsive properties of P(*n*Pr-SEMA) enable the preparation of NGs via such a precipitation polymerization in an all-aqueous system.

Fully assessing the potential of this approach requires a systematic evaluation of the synthetic control and chemical versatility. Thus, in this study, we focus on four key aspects: First, we demonstrate control over colloidal properties like size, size distribution, and crosslinking density. We examine the influence of these parameters on the temperature-dependent swelling profiles and develop a standard synthetic protocol. Second, we examine the synthetic versatility to introduce additional stimuli-responsive behavior. For this, we vary the chemical composition of the network by introducing methacrylic acid (MAA) as a functional co-monomer. The resulting additional pH-dependent swelling properties are then examined. Third, we introduce additional network degradability by using degradable crosslinkers during NG preparation. Here, we focus on the reduction-sensitive crosslinker bis(2-methacryloyloxyethyl) disulfide (DSDMA) to enable NG degradation in biological environments with changed redox potential, for example, cellular endosomes, inflamed tissues, and so forth. Fourth, we examine cytotoxicity and colloidal stability of the NGs in biologically relevant media. Overall, this systematic study establishes P(*n*Pr-SEMA)-based NGs as versatile materials for biomedical applications.

2 | Materials and Methods

2.1 | Materials

All starting materials and reagents were purchased from commercial sources and used without further purification unless otherwise stated. Tetraethylene glycol dimethacrylate (TEGDMA) and ethylene glycol dimethacrylate (EGDMA) were purchased from Sigma Aldrich. Before usage, EGDMA and TEGDMA were filtered through an Al_2O_3 column to remove any stabilizers. Ammonium persulfate (APS) and sodium dodecyl sulfate (SDS) were purchased from Merck. 2-(*n*-propyl-sulfoxide)ethyl methacrylate *n*Pr-SEMA [34] and DSDMA [41] were prepared according to literature procedures. Ultrapure water was taken from a LaboStar UV 2 water system. Air-sensitive reactions were carried out under a nitrogen atmosphere.

2.2 | Nanogel Synthesis via Precipitation Polymerization

2.2.1 | Preparation of P(*n*Pr-SEMA) Nanogels

All polymerizations were conducted in 25 mL round bottom flasks equipped with a magnetic stirring bar. In a typical reaction, 204.0 mg *n*Pr-SEMA (1 mmol) and 9.91 mg (0.03 mmol) tetraethylene glycol dimethacrylate (TEGDMA, 3 mol% w.r.t the monomer) were dissolved in 10 mL of a 0.45 mM sodium dodecyl sulfate (SDS) solution in Milli-Q water at a slightly acidic pH between 6 and 7The initiator solution was prepared by dissolving 25.5 mg ammonium persulfate (APS, 0.12 mmol) in 5 mL of Milli-Q water. Both aqueous solutions were filtered over a cellulose-mixed ester syringe filter (0.20 μm) and subsequently purged with nitrogen to remove any oxygen for 20 min while stirring with a rotation speed of 450 rpm. The reaction mixture was then placed in a preheated oil bath at 70°C. After an equilibration time of 10 min, the polymerization was started by rapidly adding 0.5 mL of the initiator solution under nitrogen atmosphere. The clear and colorless solution became turbid within the first 5 min after adding the initiator. After a reaction time of 4 h, the dispersion was cooled down to RT (see ESI for dialysis protocols).

2.2.2 | Preparation of P(*n*Pr-SEMA-*co*-MAA) Nanogels

P(*n*Pr-SEMA-*co*-MAA) NGs were prepared the same way as aforementioned, adding to the reaction mixture 2.5, 5.0, and 10.0 mol% (w.r.t. *n*Pr-SEMA) of MAA, which had been previously filtered over Al_2O_3 to remove any stabilizing agents. The pH of the reaction mixture remained in the neutral range, between 6 and 7, before and after the reaction took place (see ESI for synthetic details).

2.3 | Characterization of Nanogels

2.3.1 | Dynamic Light Scattering (DLS)

The particle size distributions were measured by DLS at 90° in multiangle round cell glass cuvettes using NICOMP nano Z3000 (Particle Sizing Systems, USA). For this, NG dispersions in water were used at a concentration of 1.0 mg/mL. The measurements were conducted in triplicates with an acquisition time of 3 min. The dispersions were filtered over cotton to remove any larger dust particles prior to the measurements. The temperature trends were measured in a temperature range of 5°C–50°C in steps of 5°C. Size and size distribution based on the intensity-weighted average diameters were computed by 9.21/E1 (9.21) of NICOMP software using Gaussian analysis. The sigmoidal curves obtained from plotting the mean diameters at each temperature were differentiated, and the temperature at the inflection point was defined as the VPTT.

2.3.2 | Turbidity Measurements for Monitoring Nanogel Degradation

Degradation studies were performed by measuring the time-dependent light scattering intensity at 90° in multiangle round cell glass cuvettes using NICOMP nano Z3000 (Particle Sizing Systems, USA). For this, 1 mg/mL dispersions of the respective NGs in PBS were prepared, and the dispersion was equilibrated in the DLS device for 2 min at 37°C. Afterward, 10 mM DTT was added to the dispersion, and the scattering intensity was monitored for 90 min.

2.3.3 | Transmission Electron Microscopy (TEM)

The morphology and size of the NGs were investigated via TME. For this, 10 μL of the respective NG dispersion (1.0 mg/mL) were placed on a carbon-coated copper grid (400 meshes, Quantifoil Micro Tools GmbH, Großlöbichau, Germany) to air-dry overnight at room temperature. The dispersions were filtered over a 0.45 μm cellulose-mixed ester syringe filter prior to the measurements. The prepared samples were measured using the TEM mode of a Hitachi scanning electron microscope (SU8030, Hitachi High-Technologies Corporation, Tokyo, Japan) with a working voltage of 30.0 kV at different magnifications. In order to evaluate the size and the size distribution of the NGs in their dry state, the diameter of around 100 individual particles of each sample was determined with the software ImageJ (version 1.53t).

2.3.4 | pH-Dependent Swelling Studies

The swelling behavior at different pH of the NGs containing 2.5, 5, and 10 mol% MAA was tested by DLS measurements. For this, a NG dispersion of 1 mg/mL was incubated in phosphate buffered solution adjusted to five different pHs (5–9). Subsequently, the size of the NGs in dispersion was measured at RT in triplicate.

2.3.5 | Nanoparticle Tracking Analysis (NTA)

NTA studies were conducted to investigate the NGs' behavior in complex biological fluids. Particle size distribution in fetal bovine serum and bovine plasma with different incubation times was determined by NTA using a NanoSight NS500 system (Malvern Technologies, Malvern, UK) configured with a 488 nm laser and a high-sensitivity scientific CMOS camera. The preparation of samples involved diluting a 1 mg/mL dispersion of the

respective NG in Milli-Q water with serum or plasma (1:5). After three-time points (0 day, 1 day, and 7 days), the samples were diluted with filtered Milli-Q water (1:200). NG dispersions in water were used as control. Data analysis was conducted using NTA 3.4 software with a detection threshold of 20.

2.3.6 | Cytotoxicity

The compounds' effect on the cell viability was assessed using the Cell Counting Kit-8 (CCK-8) from Sigma Aldrich according to the manufacturer's instructions. L929 fibroblasts (DSMZ no: ACC 2, Leibniz Institute DSMZ—German Collection of Microorganism and Cell Cultures) were cultured in Dulbecco's Modified Eagle Medium (DMEM), high glucose supplemented with L-Glutamine, 10.000 U mL^{-1} Penicillin–Streptomycin, and 10% Fetal Bovine Serum (all from Gibco BRL, Eggenstein, Germany). For the assay, 90 µL of L929 cells in DMEM were seeded in the inner wells of a 96-well plate (50.000 cells mL^{-1}) and incubated overnight at 37°C and 5% CO_2. In the outer wells, 90 µL of DMEM without cells was added for background subtraction. 10 µL of the sample (in sterile MilliQ water) were added in serial dilutions, including a positive (1% SDS) and a negative control (H_2O, medium). After the addition of the compounds, the cells were incubated for another day before 10 µL of CCK-8 solution was added to each well. After 3 h of incubation, absorbance was measured (450 nm/ 630 nm) with a Tecan plate reader (Infinite pro200, TECAN-reader Tecan Group Ltd., Männedorf, Switzerland). The whole experiment was repeated three times. To calculate the cell viability, the non-treated control was set to 100% and the values for the treated cells were normalized to the non-treated control. The background signal was subtracted using the Excel software. Origin was used to plot the mean with the standard deviation of all three assay runs for all compound concentrations. The results were subjected to an analysis of variance with multiple comparisons (one-way ANOVA and Dunnett's test) with a level of significance (α) of 0.05. Statistical analysis was performed on GraphPad Prism software (v.9.0.1, GraphPad, La Jolla, CA, USA).

3 | Results and Discussion

3.1 | Poly(*n*Pr-SEMA)-Based Nanogels: Influence of Synthetic Parameters on Colloidal Features and Thermo-Responsive Swelling Profiles

NGs based on 2-(*n*-propyl-sulfoxide ethyl) methacrylate (*n*Pr-SEMA) were prepared via free radical precipitation polymerization in water. We first developed a synthetic standard protocol that is suitable for the incorporation of functional co-monomers. For this, we optimized the synthetic process using only *n*Pr-SEMA as monomer without any further co-monomers. The influence of crosslinker type, crosslinker concentration, and surfactant concentration was investigated to determine the level of control over crosslinking density, NG size, and swelling behavior of P(*n*Pr-SEMA) NGs (see Scheme 1).

The mechanism of particle formation is based on the temperature-sensitive phase separation behavior of *n*Pr-SEMA based polymers in aqueous solutions. The precipitation polymerization begins in a homogenous solution of monomer, crosslinker, and surfactant at 70°C (T>LCST of P(*n*Pr-SEMA) polymers). After initiation, short, oligomeric chains precipitate out of the solution as they reach a critical chain length, forming precursor particles. These phase-separated nuclei grow by aggregation and further reaction with monomers and crosslinkers to eventually form stable colloids [42].

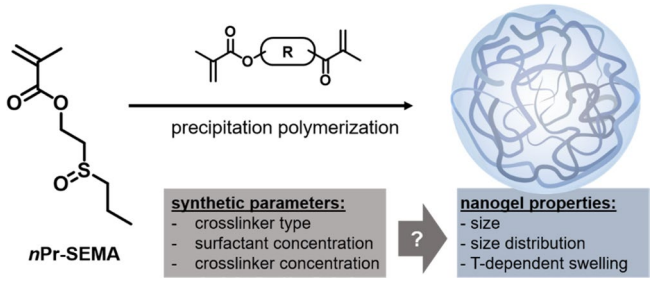

SCHEME 1 | Development of a standard synthetic procedure for the free radical precipitation polymerization of *n*Pr-SEMA in water. Examining the influence of synthetic parameters on the resulting NG properties.

3.1.1 | Choosing Suitable Crosslinkers

In NGs, widely used crosslinkers are α,ω-functionalized (oligo) ethylene glycol di(meth)acrylates. In these bifunctional monomers, the number of ethylene glycol units between methacrylate end groups determines crosslinker hydrophilicity and the length of the connection between two polymer chains. During aqueous precipitation co-polymerizations, such variations can impact the introduction of the crosslinker into the growing polymer network, thus affecting crosslinking efficiency and crosslinker distribution. Thus, the impact of crosslinker structure on NG properties needs to be determined.

For this, we performed precipitation co-polymerizations of *n*Pr-SEMA with 3 mol% of ethyleneglycol dimethacrylate (EGDMA) and tetraethyleneglycol dimethacrylate (TEGDMA) (ESI, Table S4). We found that crosslinking was successful for TEGDMA, while sufficient crosslinking failed when using EGDMA. This was assessed by monitoring the light scattering intensity at different temperatures (ESI, Figure S1). At temperatures above the cloud point temperature of P(*n*Pr-SEMA) (T > 30°C), both dispersions showed a high scattering intensity, thus indicating the presence of colloidal particles. Upon cooling, the scattering intensity of the TEGDMA sample decreased but still showed pronounced turbidity. This suggests the existence of crosslinked temperature-sensitive NGs that swell upon cooling. In contrast, scattering intensity of the EGDMA sample dropped to zero upon cooling. This suggests, that crosslinking was not efficient and non-crosslinked precipitates dissolve into linear polymer chains that give a transparent solution (ESI, Figure S1). Based on these results, we chose TEGDMA as a suitable crosslinker for our standard synthetic protocol.

3.1.2 | Controlling Nanogel Size by Surfactant Concentration

The thermo-induced precipitation polymerization process is affected by (ionic) surfactants [43]. In our studies, we use SDS, that

acts as a stabilizing agent for the growing nuclei, decreasing interfacial tension while the charged head groups improve electrostatic stabilization [44, 45]. The SDS concentration influences the number and size of precursor particles during the nucleation stage. Thus, higher SDS concentrations increase the number of primary particles and eventually result in smaller NGs due to monomer distribution across more polymerization sites [46]. As a result, the size of the final NGs can be controlled by changing the SDS concentration [44]. To assess this influence, we prepared P(*n*Pr-SEMA) NGs using SDS as surfactant and varied the SDS concentration from 0.3 to 1.2 mM. During this test, TEGDMA was used as the crosslinking agent with a constant concentration of 3 mol% w.r.t. the monomer. The size of the obtained NGs was then examined by DLS. Since the networks are thermo-responsive, particle size was determined below and above the phase transition temperature of the linear P(*n*Pr-SEMA), that is, at 5°C and 50°C, respectively [34]. At both temperatures, an apparent decrease in particle size with increasing SDS concentration was observed (Figure 1). The average hydrodynamic diameter (d_h) of three independently synthesized NGs decreased by 50% from 408 nm (0.3 mM) to 198 nm (1.2 mM) at 5°C and from 184 nm (0.3 mM) to 107 nm (1.2 mM) at 50°C. Further increasing c(SDS) to 1.5 mM did not result in particle formation, thus suggesting a concentration of 1.2 mM as the upper limit in this synthetic procedure.

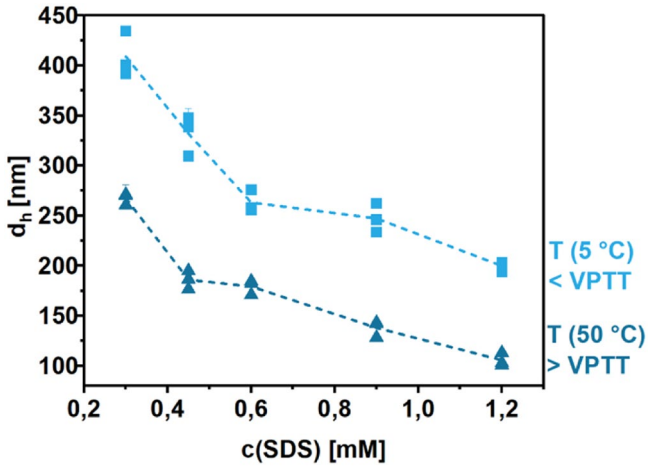

FIGURE 1 | Controlling NG size by surfactant concentration. P(*n*Pr-SEMA) NGs (3 mol% TEGDMA) decrease in size as the c(SDS) increases. Values were obtained from DLS on P(*n*Pr-SEMA) NG dispersions in water at temperatures of 5°C and 50°C.

Comparing the sizes at 5°C and 50°C, the NGs are larger at lower temperatures for all SDS concentrations. This can be attributed to their temperature-responsive properties which are governed by the balance of polymer-polymer vs. polymer-water interactions [47]. At lower temperatures, the P(*n*Pr-SEMA) NGs are swollen due to the strong solubilization of the sulfoxide groups. Above their volume phase transition temperature (VPTT), hydrogen bonds between sulfoxides and water break, while dispersive hydrophobic forces between the alkyl side groups increase. As a result, the networks collapse into smaller, less hydrated colloids. To determine the VPTT, we measured the hydrodynamic diameter across a temperature range from 5°C to 50°C and found that the NGs exhibited typical sigmoidal (de)-swelling profiles (Figure 2a) with VPTTs between 30°C and 35°C. Notably, the crosslinked networks exhibit a broader phase transition range compared to the distinct T*cp* of the corresponding linear polymers [34]. This can be explained by an inhomogeneous length distribution of free segments between crosslinking points [48]. The corresponding radial gradient in crosslinking density is the result of the precipitation polymerization and leads to a denser crosslinked core and looser crosslinked corona with longer dangling chains [42, 49, 50]. Nevertheless, the VPTTs of the P(*n*Pr-SEMA) NGs closely align with the corresponding linear polymer analogs (36°C) [34] Observed variations (Figure 2b,c) between different crosslinking densities can be attributed to subtle changes in the reaction conditions, influencing the morphology and, consequently, the phase transition behavior of the NGs.

In addition to particle size in dispersion, morphology and size in the dried state were examined by TEM (ESI, Figure S2). TEM images reveal the formation of well-defined spherical-shaped NGs with monomodal narrow particle size distributions, showing good control of the particle preparation process. The diameter of dry NGs decreased with increasing SDS concentrations: 215 ± 30 for 0.3 mM, 139 ± 21 nm for 0.45 mM, 127 ± 12 nm for

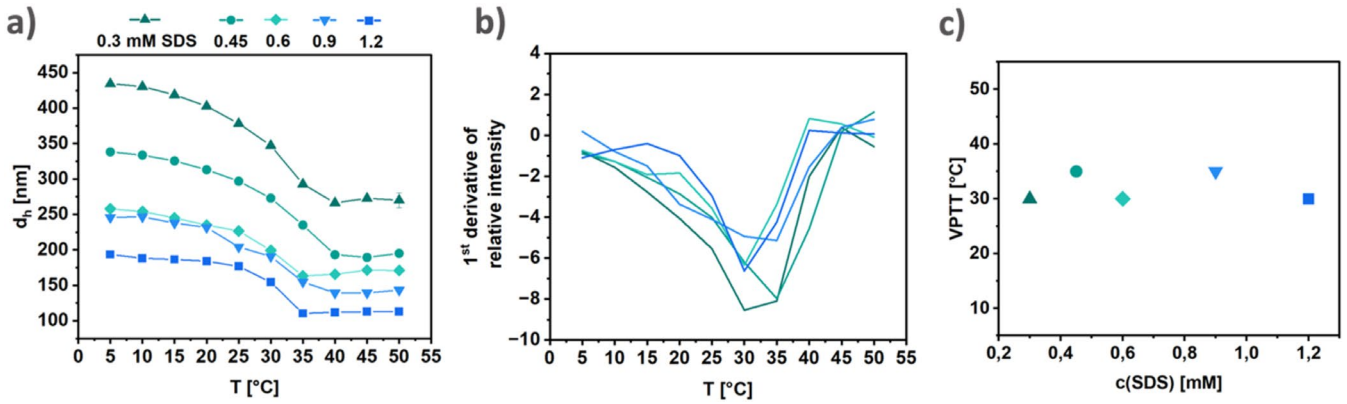

FIGURE 2 | All NGs show similar thermo-responsive properties that are independent of the used SDS concentration in their preparation. (a) Typical sigmoidal deswelling profile of thermo-responsive P(*n*Pr-SEMA) NGs show that NG size decreases above a transition temperature. (b) First-order derivative of the sigmoidal swelling profiles gives access to VPTT values between 30°C and 35°C. (c) VPTT is independent of the used SDS concentration in the NG preparation.

0.6 mM, 95 ± 18 nm for 0.9 mM, and 56 ± 11 nm for 1.2 mM (ESI, Figure S3). These results are consistent with the sizes of the collapsed particles obtained by DLS, suggesting good control over NG size by changing the surfactant concentration. Based on these examinations, 0.45 mM SDS was identified as the standard concentration for all subsequent NG syntheses (Figure 3).

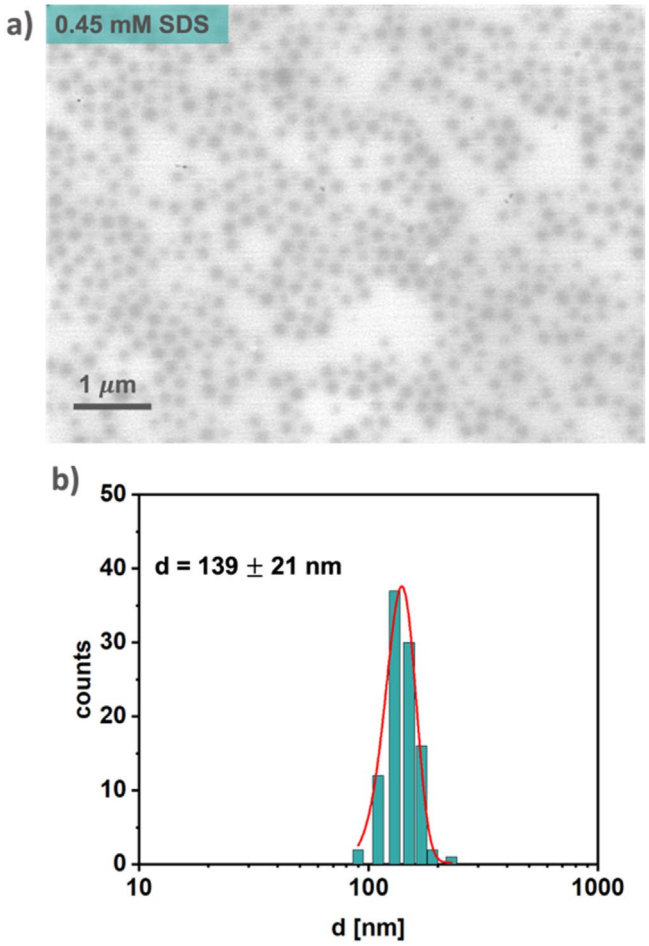

FIGURE 3 | P(*n*Pr-SEMA) NGs synthesized with 0.45 mM SDS show a monomodal narrow size distribution and well-defined spherical morphology. (a) TEM image and (b) corresponding size distribution of the P(*n*Pr-SEMA) NGs synthesized using 0.45 mM of SDS. The size distribution was determined by evaluating 100 particles in the dry state, and the histogram was fitted by a Gaussian curve fit.

We have demonstrated that particle size can be controlled efficiently using SDS. The correlation between particle size and the concentration of SDS used during the synthesis has been previously reported for thermo-responsive micro−/nanogel systems based on P(NIPAm) [43, 44, 51–53] and P(OEGMA) [25]. This indicates that our system behaves similar to established materials, thus reinforcing the robustness of the applied synthetic method. Furthermore, it provides confidence that existing knowledge such as scalability of precipitation polymerizations [54] might also be applicable to our system.

3.1.3 | Tuning the Degree of Swelling via Crosslinker Concentration

In a NG, the crosslinking density influences mesh size and, therefore, the swelling degree of the network: If less crosslinker is used, the P(*n*Pr-SEMA) chains between adjacent crosslinking points are assumed to be longer, resulting in larger mesh sizes and increased network flexibility [55]. Such an increased flexibility results in a larger ability to swell.

To control swelling by crosslinker concentration, we prepared 5 different NGs with varying amounts of TEGDMA (2, 3, 4,5, and 7.5 mol%). Temperature-dependent size measurements of the NGs revealed the anticipated sigmoidal curves (Figure 4a). Below the VPTT, NG size increases with decreasing temperature. The extent of this effect depends on the crosslinker concentration and size increases with decreasing crosslinking density. Above the VPTT, all NGs collapse to a similar size since they were prepared under similar conditions, that is, with the same amount of SDS.

Quantification of this effect uses the degree of swelling (DGS), which can be defined as the ratio between the particle volume in the swollen state ($V_{swollen}$) and the particle volume in the collapsed state ($V_{collapsed}$). In the sigmoidal swelling curves (Figure 4b), the DGS was normalized to the averaged collapsed volume of each NG and shows that swelling decreases with

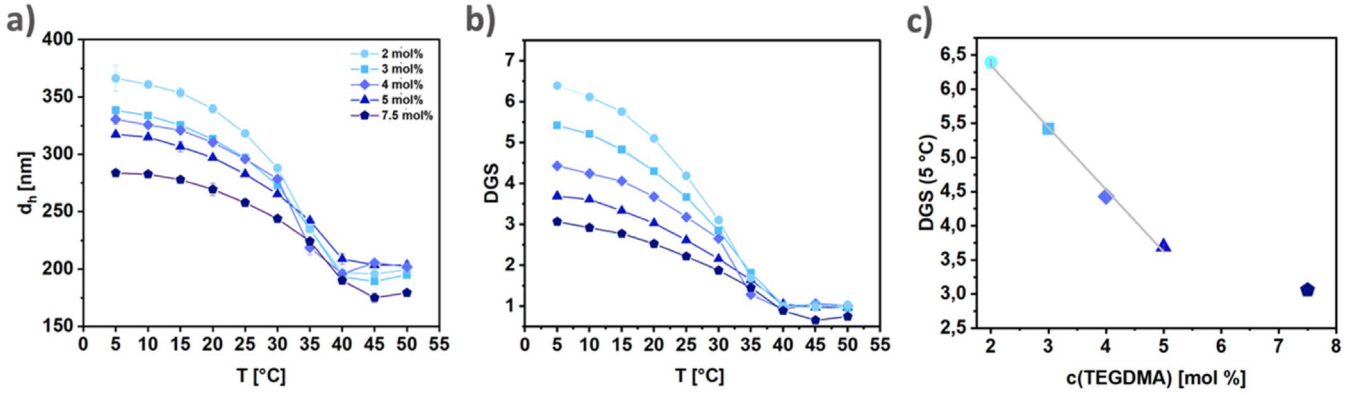

FIGURE 4 | Swelling of P(*n*Pr-SEMA) NGs can be controlled by crosslinking density. (a) Lower crosslinker concentrations increase the size of NGs below their VPTT. (b) Swelling curves of DGS vs. temperature give a quantitative assessment of the swelling properties. Here, DGS is normalized to the collapsed volume at T>VPTT to ensure comparability between NGs. (c) Correlation between the maximum DGS at 5°C and crosslinking density c(TEGDMA) shows a linear dependency for c(TEGDMA) up to 5 mol%.

increasing crosslinker concentration. Here, NGs with 2 mol% crosslinker swell more than twice as NGs with 7.5 mol% crosslinker. Comparing the maximum swollen state at 5°C of the different NGs, we found DGS_{max} to decrease linearly with increasing TEGDMA concentrations up to 5 mol% (Figure 4c). Overall, all NGs exhibited a VPTT close to 35°C, showing that the crosslinking density does not influence their temperature-sensitivity (ESI, Figure S4). This suggests good control of the network's temperature-dependent swelling capacity through variation of the crosslinker concentration. These results align with comparable thermo-responsive microgels based on P(NIPAm) [56]. In such systems, it is known that swelling capacity and size decrease with increasing concentrations of crosslinker (e.g., *N,N′*-methylenebisacrylamide (BIS) with 2, 5, 15 mol%), without changing the VPTT [56]. A comparison of VPTTs and swelling capacities from selected P(NIPAm) and P(OEGMA) based micro−/nanogels with comparable crosslinking densities is presented in the SI (Table S9).

3.2 | Introducing Additional pH Responsiveness: Copolymerization With Methacrylic Acid Gives Access to Double-Responsive Swelling Profiles

To expand the NGs' stimuli-responsive properties beyond their thermo-responsiveness, co-monomers with functional groups can be incorporated. pH-responsiveness can be achieved by incorporating basic (cationic) or acidic (anionic) monomers into the polymer network. Among those, anionic polymers generally exhibit lower cytotoxicity than cationic materials, which show strong, pH-dependent interactions with negatively charged cell membranes. Thus, we have focused on anionic methacrylic acid (MAA) as a model co-monomer to demonstrate the possibility of adding another stimuli-responsive feature. Generally, MAA is well established as co-monomer in NG synthesis and allows multiple ways of interactions (H-bond donor, H-bond acceptor, electrostatic and van der Waals interactions), thus offering potential for a variety of loading applications, that is, the electrostatic entrapment of oppositely charged biomacromolecules.

The copolymerization of *n*Pr-SEMA with methacrylic acid (MAA) leads to a double-stimuli responsive swelling behavior, that is, sensitive to changes in temperature and pH. In this case, protonation/deprotonation of MAA units governs their aqueous solubility and the corresponding network swelling [57]. At pH values above pKa (MAA) the anionic groups promote swelling due to increased osmotic pressure in the network [55, 58, 59]. For pH < pKa (MAA), protonated MAA groups are comparably hydrophobic, which decreases network swelling. Most importantly, these properties are strongly coupled to the thermo-responsive behavior since the addition of hydrophilic or hydrophobic co-monomers is known to shift the VPTT of polymer NGs [60]. We assume that the presence of hydrophilic anionic groups at high pH will shift the VPTT to higher temperatures. This effect is known to increase with the amount of hydrophilic co-monomers [61]. In contrast, the presence of hydrophobic protonated MAA groups at low pH will shift the VPTT to lower temperatures [61]. Thus, the incorporation of MAA co-monomers will offer access to a double stimuli-responsive swelling profile where pH can be used to control the temperature response.

To realize such a complex swelling profile, we prepared a set of P(*n*Pr-SEMA) NGs with varying contents of MAA, that is, 2.5, 5, and 10 mol% w.r.t. the *n*Pr-SEMA monomer. Synthesis of these NGs followed our previously developed standard procedure but included the respective amounts of MAA as co-monomer feed (see ESI, Table S7). To determine the incorporated amount of MAA in all NGs, potentiometric titrations were conducted on all NGs (see ESI, Figure S5). The actual incorporation of MAA was close to the expected values: 2.8 mol% for 2.5 mol%, 4.3 mol% for 5 mol%, and 16.4 mol% for 10 mol%. These experiments demonstrated the quantitative incorporation of MAA in all NGs, thus showing good control over network composition by the precipitation polymerization method. For all NGs, temperature-dependent and pH-dependent swelling profiles were studied by DLS and compared to the pure P(*n*Pr-SEMA) NGs.

First, we assessed the temperature-dependent swelling of the NGs at two fixed pH values. Here, we used pH 8 to ensure complete deprotonation of all MAA groups and pH 5 to promote partial MAA protonation. At pH 8, the NGs remain swollen over a wide temperature range, and the overall swelling increases with the amount of MAA (ESI, Figure S6a). In addition, all NGs show a less pronounced temperature-dependence than the native *n*Pr-SEMA NGs. We suggest that the high hydrophilicity of the deprotonated MAA groups shifts the VPTT to much higher temperatures. Since this effect scales with the amount of hydrophilic MAA groups, no temperature-dependent swelling is observed up to $T = 60$°C for NGs with 5 and 10 mol% MAA. For NGs with 2.5 mol%, the onset of a temperature-induced collapse can be seen between 55°C and 60°C. In contrast, at pH 5, protonation of the carboxylic acid groups increases the network's overall hydrophobicity, thus shifting the VPTT to lower values (ESI, Figure S6b,c). A linear trend is observed between the decreasing VPTT and increasing MAA content (Figure 5a).

Second, we assessed the pH-dependent swelling of NGs at a fixed temperature of $T = 25$°C. For this, we dispersed the different NGs in phosphate buffers with pH values ranging from pH 5 to 9 and measured the corresponding hydrodynamic diameter (d_h) by DLS. Figure 5b indicates a pH-dependent phase transition between a collapsed state at pH 5 and a swollen state above pH 6. This transition is more pronounced for the NGs with higher MAA contents: For NGs with 10 mol% MAA, d_h increases from 326 nm at pH 5 to 458 nm at pH 6. For NGs with 2.5 and 5 mol% MAA, d_h changes from around 200 nm, to around 300 nm at pH 6. Above pH 6 further increasing the pH does not affect the swelling anymore. Below pH 5, redispersion of NGs resulted in aggregation. This can be explained by protonation of the carboxylic acid groups, which increases their hydrophobicity. In addition, the high ionic strength in the buffer reduces the osmotic swelling. In combination, both effects can cause aggregation of the collapsed NGs.

3.3 | Degradability

Triggered NG degradation is important to release (physically) entrapped payloads and to clear resulting NG fragments from the body. To introduce network degradability, labile crosslinkers are established to be cleaved as response to a specific biological

stimulus. In our case, we targeted changes in the redox potential that can occur due to reactive oxygen species in inflamed tissue and wounds or due to high cytosolic glutathione contents in tumor cells [62–64]. To enable network cleavage in these scenarios, we used a crosslinker with a disulfide bond, that is, bis(2-methacryloyloxyethyl) disulfide (DSDMA) (Figure 6a). Due to the hydrophobic nature of this crosslinker, low solubility might cause deviations between the actual crosslinking density and the feed ratio. To address this challenge, we introduced an excess of 5 mol% (w.r.t. the monomer) of DSDMA. The obtained particles were smaller than those crosslinked with TEGDMA. Nevertheless, DLS and TEM revealed formation of particles with a narrow size distribution and similar thermo-responsive behavior than their non-degradable counterparts (ESI, Figures S7 and S8). To estimate the amount of DSDMA actually incorporated into the NGs, we compared the DGS of DSDMA-NGs to the correlation between DGS and crosslinker content in the TEGDMA-NGs (Figure 4c). Here, a $DGS_{(5°C)} = 6$ for the DSDMA-NGs (ESI, Figure S9a) suggests a crosslinking density of around 2.3 mol% (ESI, Figure S9b).

Crosslinker cleavage was tested by incubating the NGs with 10 mM dithiothreitol (DTT) as reducing agent in PBS at pH 7.4 (Figure 6a). Resulting NG degradation was monitored by turbidity measurements. In such experiments, an overall reduction of turbidity can be used to jointly monitor two possible NG degradation pathways: First, crosslinker cleavage causes swelling of the NGs due to a reduction of mesh size. In this case, scattering contrast decreases. Second, further cleavage of DSDMA leads to NG fragmentation into smaller pieces that scatter less [65]. For all ionic and non-ionic NGs that contain DSDMA, a significant reduction in turbidity was observed compared to the non-degradable control NGs crosslinked with TEGDMA. The decrease in turbidity is more pronounced for the MAA-containing NGs than for the pure $P(n\text{Pr-SEMA})_{dg}$ NGs (Figure 6b). This may be attributed to an enhanced swelling of the anionic NGs in PBS, which favors degradation. The degradation profile is, however, not influenced by the degree of ionization since all NGs containing 2.5, 5, and 10 mol% of MAA show similar profiles. These results show the potential for triggered release in specific biological microenvironments with high glutathione

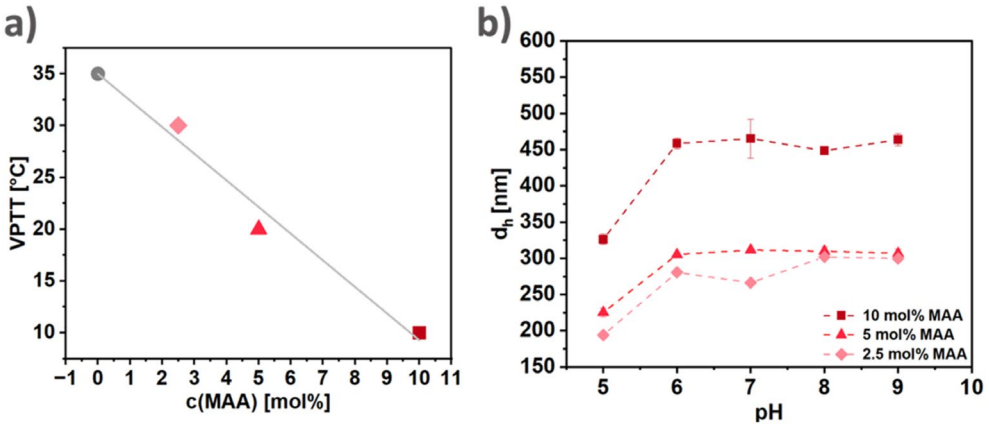

FIGURE 5 | Figure of P(*n*Pr-SEMA-*co*-MAA) NGs show double-responsive swelling behavior due to a combination of pH- and temperature-responsive properties (a) At pH ≤ pKa(MAA), the VPTT can be controlled by the amount of MAA groups in the network: For pH 5, VPTT decreases linearly with increasing c(MAA). (b) Below the VPTT of P(*n*Pr-SEMA) ($T = 20°C$), NG swelling is pH-dependent. For all experiments, the P(*n*Pr-SEMA-co-MAA) NGs containing 2.5, 5, and 10 mol% of MAA were incubated in aqueous phosphate buffers at different pH values, and their size was determined by DLS.

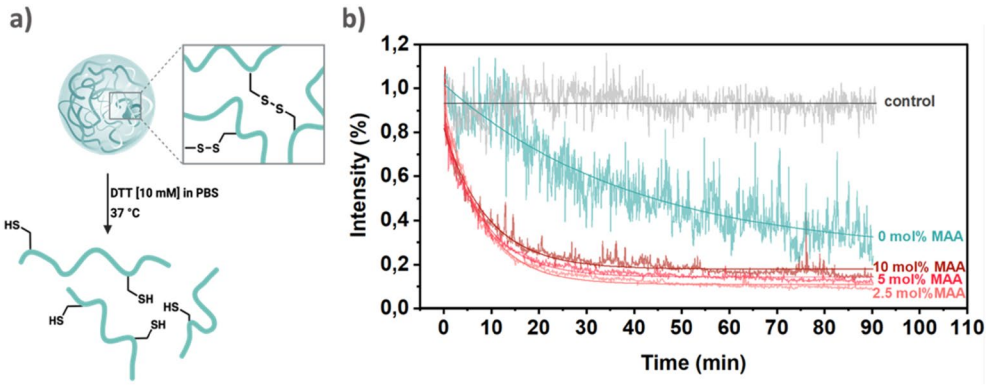

FIGURE 6 | NG degradation can be induced by cleaving disulfide-based crosslinking points in a reductive environment. (a) Schematic degradation of the P(*n*Pr-SEMA) NGs that contain DSDMA as disulfide-based crosslinker. (b) $P(n\text{Pr-SEMA-}co\text{-MAA})_{dg}$ NGs degrade faster than non-ionic $P(n\text{Pr-SEMA})_{dg}$ NGs. Control experiments were performed with non-degradable NGs in the presence of DTT. The curve fit was performed with OriginPro using the ExpDec1 function.

concentrations, that is, internal cellular delivery or tumor microenvironments [62, 66].

3.4 | Colloidal Stability in Biological Media

The multi-stimuli-responsive swelling (i.e., pH-responsive and temperature-responsive) and the reductive degradation make P(*n*Pr-SEMA) NGs promising candidates for biomedical applications. However, to fully exploit these properties, the NGs need to be colloidally stable in biological media. In such environments, the interaction of particles with proteins can lead to the formation of a protein corona, which can induce NG agglomeration [67]. In our case, we assume that this corona formation is limited due to the protein-repellent character of the sulfoxide-side groups [38]. In such a scenario, the size of the NGs should not change drastically in the presence of complex protein mixtures. To assess this behavior in complex biological media, we diluted aqueous dispersions of pure P(*n*Pr-SEMA) and anionic P(*n*Pr-SEMA-*co*-MAA) (10 mol% MAA) in bovine serum and plasma (20% vol/vol) and incubated these for up to 7 days. NTA was used to determine the hydrodynamic size immediately after dilution, after 1 day, and after 1 week. For the non-ionic *n*Pr-SEMA NGs, the size remained similar over 7 days in all three media (Figure 7). In contrast, for the ionic P(*n*Pr-SEMA-*co*-MAA-10) NGs, the size immediately increased from 177 nm in water to 366 nm in plasma and 345 nm in serum (Figure 7b,c). This suggests the adsorption of proteins from the biological fluids, probably due to a combination of electrostatic interactions and hydrogen bonding with the MAA groups in the NGs. In addition to such a potential stronger interaction, a higher degree of swelling compared to the non-ionic P(*n*Pr-SEMA) nanogels could enhance the accessibility to more hydrophobic sites within the polymer network, thus also favoring protein adsorption [68]. Further investigations to optimize the nanogels design could focus on achieving loading through electrostatic interactions while maintaining the low fouling properties of the sulfoxide moieties. However, all dispersions remained stable without the formation of larger aggregates in either of the different media. Thus, we assume that the sulfoxide side groups can successfully limit protein adsorption to a level that does not interfere with colloidal stability.

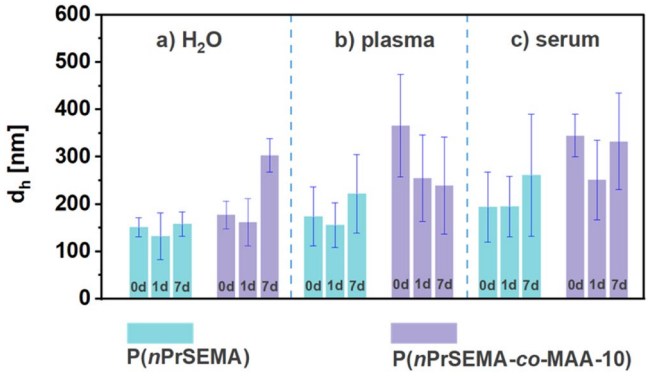

FIGURE 7 | The NG dispersions remain colloidally stable in different biologically relevant media for up to 7 days. Nanoparticles Tracking Analysis (NTA) shows the diameter of P(*n*Pr-SEMA) and P(*n*Pr-SEMA-*co*-MAA) NGs in (a) water, (b) fetal bovine serum, and (c) bovine plasma.

3.5 | Cytotoxicity

While the colloidal stability of the NGs suggests good physical compatibility with biological media, the biological interaction with actual living cells needs to be examined, too. To determine potential toxic effects of the NGs, cell viability tests were performed on L929 fibroblasts. Figure 8 depicts the cell viability of non-degradable P(*n*Pr-SEMA) NGs with varying amounts of MAA (0, 2.5, 5, 10 mol% MAA) and degradable P(*n*Pr-SEMA) NGs crosslinked with DSDMA. As can be seen, all P(*n*Pr-SEMA)-based NGs displayed high cell viability for concentrations up to 1000 μg/mL after 24 h. These results suggest that the established biocompatibility of polymers with methyl sulfoxide side groups translates to sulfoxide side groups with larger *n*-propyl side groups. Thus, increasing the alkyl length to provide a temperature-responsive behavior does not significantly diminish the compatibility with biological systems.

4 | Conclusion

We developed a synthetic platform for the preparation of multi-responsive polysulfoxide NGs. Our approach exploits the temperature-sensitivity of a polymethacrylate with *n*-propyl sulfoxide side groups P(*n*Pr-SEMA) to access well-defined NGs by precipitation polymerization. With this, we transfer the inherent hydrophilicity of sulfoxide-containing polymethacrylates to crosslinked NGs. As a result, the final materials combine temperature-sensitivity with high colloidal stability and low cellular toxicity.

The temperature-induced precipitation polymerization in water allows precise control over particle size and crosslinking without the need for organic solvents. Through the incorporation of ionizable MAA as a co-monomer, we varied the chemical composition of the crosslinked polymer network. As a result, we established a NG library with double stimuli-responsiveness, that is, thermo-responsive behavior and pH-sensitivity. The additional incorporation of a disulfide-based crosslinker enables reduction-triggered degradation of the colloidal particles, which is especially promising for site-specific delivery of therapeutic

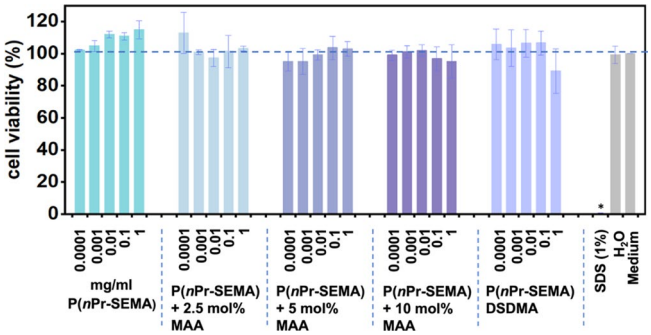

FIGURE 8 | High viability of L929 cells is observed after being treated with *n*Pr-SEMA NGs with varying MAA contents and *n*Pr-SEMA NGs crosslinked with DSDMA. Viability (mean ± SD, $n = 3$) was assessed via the CCK-8 assay after exposure to the different NGs at five concentrations (0.0001–1 mg/mL) for 24 h. SDS (1%) served as the positive control and medium, H_2O as the negative control. An asterisk denotes statistical difference ($p < 0.0001$) with respect to the control group after Dunnett's test.

cargoes. All NGs displayed low cytotoxicity across different network compositions, suggesting good biocompatibility of the system. Studies on colloidal stability in complex biological fluids indicate the potential for protein-repellent properties of the *n*Pr-SEMA sulfoxide moieties.

The successfully developed synthetic method to transfer of sulfoxide-based polymers into crosslinked NGs offers control over colloidal and chemical properties that are comparable to established PNIPAm or POEGMA-based materials. Thus, these fundamental studies on the chemical platform serve as foundation for the development of new colloidal materials, that use the unique properties of sulfoxides to tailor NG properties to specific applications. In this context, it is interesting to study the hydrophilicity-induced low-fouling properties of the polysulfoxide NGs. This makes them promising materials for the coating of medical devices, targeted drug delivery, or biosensing [38]. Here, the demonstrated chemical versatile of our synthetic platform is promising to adjust the NG properties to specific applications. For example, introducing additional responsiveness could be used to direct specific cargoes (e.g., antitumoral and antimicrobial agents, fluorescent biomarkers) toward reductive microenvironments [38] or tissues with pH gradients [69] (e.g., tumors, infections). Despite their hydrophilicity, the polar polysulfoxides also show unique interactions with proteins (e.g., acting as folding stabilizers/cryoprotectants [37]) or with biological membranes (e.g., acting as penetration enhancers [70]).

Other possibilities of this platform include the introduction of additional functionalities to further tune the NGs' swelling profile and the networks' interactions with cargoes. For example, the temperature-responsive properties can be precisely adjusted further by copolymerizing *n*Pr-SEMA with monomers containing other alkyl groups at the sulfoxide. Here, shorter, more hydrophilic, groups (Me-SEMA) are assumed to increase the VPTT, whereas longer or branched, more hydrophobic, alkyl groups (e.g., *i*Pr-SEMA) are known to decrease the VPTT. Additional functionalities could include basic moieties for cationic interactions, zwitterionic groups, or sulfones, imparting redox responsiveness in the polymer backbone.

Overall, the synthetic versatility and control of this approach gives access to NGs that are interesting alternatives to long-established colloidal nano−/microgels based on polymers like poly(*N*-isopropylacrylamide) (PNIPAm [71, 72]), POEGMA [73, 74], or poly(*N*-vinylcaprolactam) (PNVCL) [75, 76]. Here, further investigations are needed to examine whether the highly-polar sulfoxide groups cause properties that deviate from the old established microgel materials, for example, changes in cellular uptake, protein corona, and so forth.

Acknowledgments

We would like to acknowledge the assistance of the Core Facility BioSupraMol supported by the DFG. C.L-.I. acknowledges Xunta de Galicia (Conselleria de Cultura, Educacion e Ordenacion Universitaria) for a postdoctoral fellowship (ED481-B202-1008). S. K. acknowledges the German academic exchange program (DAAD) for the scholarship granted for her PhD studies (Funding programme number: 57507871, personal reference number: 91765401).

References

1. A. Vashist, G. Perez Alvarez, V. Andion Camargo, et al., "Recent Advances in Nanogels for Drug Delivery and Biomedical Applications," *Biomaterials Science* 12, no. 23 (2024): 6006–6018, https://doi.org/10.1039/D4BM00224E.

2. T. Shi, D. Kou, L. Gao, Y. Xue, S. Zhang, and W. Ma, "One-Dimensional Responsive Photonic Crystals Assembled by Polymer Nanogels and TiO2 Nanoparticles for Rapid Detection of Glucose," *ACS Applied Nano Materials* 7, no. 3 (2024): 3116–3128, https://doi.org/10.1021/acsanm.3c05440.

3. A. Beloqui, A. Y. Kobitski, G. U. Nienhaus, and G. Delaittre, "A Simple Route to Highly Active Single-Enzyme Nanogels," *Chemical Science* 9, no. 4 (2018): 1006–1013, https://doi.org/10.1039/C7SC04438K.

4. S. Hajebi, N. Rabiee, M. Bagherzadeh, et al., "Stimulus-Responsive Polymeric Nanogels as Smart Drug Delivery Systems," *Acta Biomaterialia* 92 (2019): 1–18, https://doi.org/10.1016/j.actbio.2019.05.018.

5. D. Klinger, E. M. Aschenbrenner, C. K. Weiss, and K. Landfester, "Enzymatically Degradable Nanogels by Inverse Miniemulsion Copolymerization of Acrylamide With Dextran Methacrylates as Crosslinkers," *Polymer Chemistry* 3, no. 1 (2012): 204–216, https://doi.org/10.1039/C1PY00415H.

6. A. Gruber, L. Navarro, and D. Klinger, "Dual-Reactive Nanogels for Orthogonal Functionalization of Hydrophilic Shell and Amphiphilic Network," *Soft Matter* 18, no. 14 (2022): 2858–2871, https://doi.org/10.1039/d2sm00116k.

7. A. F. Thünemann, A. Gruber, and D. Klinger, "Amphiphilic Nanogels: Fuzzy Spheres With a Pseudo-Periodic Internal Structure," *Langmuir: The Journal of the American Chemical Society* 36, no. 37 (2020): 10979–10988, https://doi.org/10.1021/acs.langmuir.0c01812.

8. A. R. Town, J. Taylor, K. Dawson, et al., "Tuning HIV Drug Release From a Nanogel-Based In Situ Forming Implant by Changing Nanogel Size," *Journal of Materials Chemistry B* 7, no. 3 (2019): 373–383, https://doi.org/10.1039/C8TB01597J.

9. W. Chen, M. Zheng, F. Meng, et al., "In Situ Forming Reduction-Sensitive Degradable Nanogels for Facile Loading and Triggered Intracellular Release of Proteins," *Biomacromolecules* 14, no. 4 (2013): 1214–1222, https://doi.org/10.1021/bm400206m From NLM.

10. S. Khizar, N. Zine, A. Errachid, and A. Elaissari, "Introduction to Stimuli-Responsive Materials and Their Biomedical Applications," in *Stimuli-Responsive Materials for Biomedical Applications, ACS Symposium Series*, vol. 1436 (American Chemical Society, 2023), 1–30.

11. M. Shahriari, M. Zahiri, K. Abnous, S. M. Taghdisi, M. Ramezani, and M. Alibolandi, "Enzyme Responsive Drug Delivery Systems in Cancer Treatment," *Journal of Controlled Release* 308 (2019): 172–189, https://doi.org/10.1016/j.jconrel.2019.07.004.

12. T. Kaewruethai, C. Laomeephol, Y. Pan, and J. A. Luckanagul, "Multifunctional Polymeric Nanogels for Biomedical Applications," *Gels* 7, no. 4 (2021): 228.

13. H. Wang, N. Tiwari, M. S. Orellano, et al., "Polyglycerol-Functionalized β-Cyclodextrins as Crosslinkers in Thermoresponsive Nanogels for the Enhanced Dermal Penetration of Hydrophobic Drugs," *Small* 20, no. 32 (2024): 2311166, https://doi.org/10.1002/smll.202311166.

14. M. Karimi, P. Sahandi Zangabad, A. Ghasemi, et al., "Temperature-Responsive Smart Nanocarriers for Delivery of Therapeutic Agents: Applications and Recent Advances," *ACS Applied Materials & Interfaces* 8, no. 33 (2016): 21107–21133, https://doi.org/10.1021/acsami.6b00371.

15. J. Bergueiro, E. A. Glitscher, and M. Calderón, "A Hybrid Thermoresponsive Plasmonic Nanogel Designed for NIR-Mediated Chemotherapy," *Biomaterials Advances* 137 (2022): 212842, https://doi.org/10.1016/j.bioadv.2022.212842.

16. T. L. Moore, L. Rodriguez-Lorenzo, V. Hirsch, et al., "Nanoparticle Colloidal Stability in Cell Culture Media and Impact on Cellular Interactions," *Chemical Society Reviews* 44, no. 17 (2015): 6287–6305, https://doi.org/10.1039/C4CS00487F.

17. S. Schöttler, K. Landfester, and V. Mailänder, "Controlling the Stealth Effect of Nanocarriers Through Understanding the Protein Corona," *Angewandte Chemie (International Ed. in English)* 55, no. 31 (2016): 8806–8815, https://doi.org/10.1002/anie.201602233.

18. R. Augustine, A. Hasan, R. Primavera, R. J. Wilson, A. S. Thakor, and B. D. Kevadiya, "Cellular Uptake and Retention of Nanoparticles: Insights on Particle Properties and Interaction With Cellular Components," *Materials Today Communications* 25 (2020): 101692, https://doi.org/10.1016/j.mtcomm.2020.101692.

19. M. Awashra and P. Młynarz, "The Toxicity of Nanoparticles and Their Interaction With Cells: An In Vitro Metabolomic Perspective," *Nanoscale Advances* 5, no. 10 (2023): 2674–2723, https://doi.org/10.1039/d2na00534d.

20. M. Ovais, S. K. Nethi, S. Ullah, I. Ahmad, S. Mukherjee, and C. Chen, "Recent Advances in the Analysis of Nanoparticle-Protein Coronas," *Nanomedicine* 15, no. 10 (2020): 1037–1061, https://doi.org/10.2217/nnm-2019-0381.

21. P. Eslami, F. Rossi, and S. Fedeli, "Hybrid Nanogels: Stealth and Biocompatible Structures for Drug Delivery Applications," *Pharmaceutics* 11, no. 2 (2019): 71, https://doi.org/10.3390/pharmaceutics11020071.

22. P. Aggarwal, J. B. Hall, C. B. McLeland, M. A. Dobrovolskaia, and S. E. McNeil, "Nanoparticle Interaction With Plasma Proteins as It Relates to Particle Biodistribution, Biocompatibility and Therapeutic Efficacy," *Advanced Drug Delivery Reviews* 61, no. 6 (2009): 428–437, https://doi.org/10.1016/j.addr.2009.03.009.

23. Y. Tian, Z. Gao, N. Wang, et al., "Engineering Poly(Ethylene Glycol) Nanoparticles for Accelerated Blood Clearance Inhibition and Targeted Drug Delivery," *Journal of the American Chemical Society* 144, no. 40 (2022): 18419–18428, https://doi.org/10.1021/jacs.2c06877.

24. J. M. W. Chan, R. J. Wojtecki, H. Sardon, et al., "Self-Assembled, Biodegradable Magnetic Resonance Imaging Agents: Organic Radical-Functionalized Diblock Copolymers," *ACS Macro Letters* 6, no. 2 (2017): 176–180, https://doi.org/10.1021/acsmacrolett.6b00924.

25. Y. Liu, Y. N. Luo, P. Zhang, W. F. Yang, C. Y. Zhang, and Y. L. Yin, "The Preparation of Novel P(OEGMA-Co-MEO2MA) Microgels-Based Thermosensitive Hydrogel and Its Application in Three-Dimensional Cell Scaffold," *Gels* 8, no. 5 (2022): 313, https://doi.org/10.3390/gels8050313.

26. D. d. M. Zanata and M. I. Felisberti, "Thermo- and pH-Responsive POEGMA-b-PDMAEMA-b-POEGMA Triblock Copolymers," *European Polymer Journal* 167 (2022): 111069, https://doi.org/10.1016/j.eurpolymj.2022.111069.

27. G. T. Kozma, T. Mészáros, I. Vashegyi, et al., "Pseudo-Anaphylaxis to Polyethylene Glycol (PEG)-Coated Liposomes: Roles of Anti-PEG IgM and Complement Activation in a Porcine Model of Human Infusion Reactions," *ACS Nano* 13, no. 8 (2019): 9315–9324, https://doi.org/10.1021/acsnano.9b03942.

28. R. d'Arcy, F. El Mohtadi, N. Francini, et al., "A Reactive Oxygen Species-Scavenging 'Stealth' Polymer, Poly(Thioglycidyl Glycerol), Outperforms Poly(Ethylene Glycol) in Protein Conjugates and Nanocarriers and Enhances Protein Stability to Environmental and Biological Stressors," *Journal of the American Chemical Society* 144, no. 46 (2022): 21304–21317, https://doi.org/10.1021/jacs.2c09232.

29. R. Pelton, "Temperature-Sensitive Aqueous Microgels," *Advances in Colloid and Interface Science* 85, no. 1 (2000): 1–33, https://doi.org/10.1016/S0001-8686(99)00023-8.

30. L. Tang, L. Wang, X. Yang, Y. Feng, Y. Li, and W. Feng, "Poly(N-Isopropylacrylamide)-Based Smart Hydrogels: Design, Properties and Applications," *Progress in Materials Science* 115 (2021): 100702, https://doi.org/10.1016/j.pmatsci.2020.100702.

31. R. Qiao, C. Fu, Y. Li, et al., "Sulfoxide-Containing Polymer-Coated Nanoparticles Demonstrate Minimal Protein Fouling and Improved Blood Circulation," *Advanced Science* 7, no. 13 (2020): 2000406, https://doi.org/10.1002/advs.202000406.

32. S. Garnier and A. Laschewsky, "Non-Ionic Amphiphilic Block Copolymers by RAFT-Polymerization and Their Self-Organization," *Colloid and Polymer Science* 284, no. 11 (2006): 1243–1254, https://doi.org/10.1007/s00396-006-1484-9.

33. P. Hennaux and A. Laschewsky, "Novel Nonionic Surfactants Based on Sulfoxides. 2. Homo- and Copolymers," *Colloid and Polymer Science* 281, no. 9 (2003): 807–814, https://doi.org/10.1007/s00396-002-0830-9.

34. D. Işık, E. Quaas, and D. Klinger, "Thermo- and Oxidation-Sensitive Poly(Meth)Acrylates Based on Alkyl Sulfoxides: Dual-Responsive Homopolymers From One Functional Group," *Polymer Chemistry* 11, no. 48 (2020): 7662–7676, https://doi.org/10.1039/D0PY01321H.

35. G. R. Ediriweera, N. J. Butcher, A. Kothapalli, et al., "Lipid Sulfoxide Polymers as Potential Inhalable Drug Delivery Platforms With Differential Albumin Binding Affinity," *Biomaterials Science* 12, no. 11 (2024): 2978–2992, https://doi.org/10.1039/D3BM02020G.

36. C. Fu, B. Demir, S. Alcantara, et al., "Low-Fouling Fluoropolymers for Bioconjugation and In Vivo Tracking," *Angewandte Chemie International Edition* 59, no. 12 (2020): 4729–4735, https://doi.org/10.1002/anie.201914119.

37. A. A. Burkey, A. Hillsley, D. T. Harris, et al., "Mechanism of Polymer-Mediated Cryopreservation Using Poly(Methyl Glycidyl Sulfoxide)," *Biomacromolecules* 21, no. 8 (2020): 3047–3055, https://doi.org/10.1021/acs.biomac.0c00392.

38. X. Xu, X. Huang, Y. Chang, et al., "Antifouling Surfaces Enabled by Surface Grafting of Highly Hydrophilic Sulfoxide Polymer Brushes," *Biomacromolecules* 22, no. 2 (2021): 330–339, https://doi.org/10.1021/acs.biomac.0c01193.

39. Y. Zhang, M. Zhang, X. Xu, et al., "Anti-Fouling Surfaces for Extracorporeal Membrane Oxygenation by Surface Grafting of Hydrophilic Sulfoxide Polymers," *Biomacromolecules* 23, no. 10 (2022): 4318–4326, https://doi.org/10.1021/acs.biomac.2c00775.

40. C. Biglione, T. M. P. Neumann-Tran, S. Kanwal, and D. Klinger, "Amphiphilic Micro- and Nanogels: Combining Properties From Internal Hydrogel Networks, Solid Particles, and Micellar Aggregates," *Journal of Polymer Science* 59, no. 22 (2021): 2665–2703, https://doi.org/10.1002/pol.20210508.

41. R. H. Utama, Y. Jiang, P. B. Zetterlund, and M. H. Stenzel, "Biocompatible Glycopolymer Nanocapsules via Inverse Miniemulsion Periphery RAFT Polymerization for the Delivery of Gemcitabine," *Biomacromolecules* 16, no. 7 (2015): 2144–2156, https://doi.org/10.1021/acs.biomac.5b00545.

42. Y. Nishizawa, H. Minato, T. Inui, T. Uchihashi, and D. Suzuki, "Nanostructures, Thermoresponsiveness, and Assembly Mechanism of Hydrogel Microspheres During Aqueous Free-Radical Precipitation Polymerization," *Langmuir: The Journal of the American Chemical Society* 37, no. 1 (2021): 151–159, https://doi.org/10.1021/acs.langmuir.0c02654.

43. B. Wedel, T. Brändel, J. Bookhold, and T. Hellweg, "Role of Anionic Surfactants in the Synthesis of Smart Microgels Based on Different Acrylamides," *ACS Omega* 2, no. 1 (2017): 84–90, https://doi.org/10.1021/acsomega.6b00424 From NLM.

44. M. Andersson and S. L. Maunu, "Structural Studies of Poly(N-Isopropylacrylamide) Microgels: Effect of SDS Surfactant Concentration in the Microgel Synthesis," *Journal of Polymer Science Part B: Polymer Physics* 44, no. 23 (2006): 3305–3314, https://doi.org/10.1002/polb.20971.

45. X. Wu, R. H. Pelton, A. E. Hamielec, D. R. Woods, and W. McPhee, "The Kinetics of Poly(N-Isopropylacrylamide) Microgel Latex Formation," *Colloid and Polymer Science* 272, no. 4 (1994): 467–477, https://doi.org/10.1007/BF00659460.

46. K. von Nessen, M. Karg, and T. Hellweg, "Thermoresponsive Poly(N-Isopropylmethacrylamide) Microgels: Tailoring Particle Size by Interfacial Tension Control," *Polymer* 54, no. 21 (2013): 5499–5510, https://doi.org/10.1016/j.polymer.2013.08.027.

47. Y. H. Bae, T. Okano, and S. W. Kim, "Temperature Dependence of Swelling of Crosslinked Poly(N,N′-Alkyl Substituted Acrylamides) in Water," *Journal of Polymer Science Part B: Polymer Physics* 28, no. 6 (1990): 923–936, https://doi.org/10.1002/polb.1990.090280609.

48. D. Klinger and K. Landfester, "Stimuli-Responsive Microgels for the Loading and Release of Functional Compounds: Fundamental Concepts and Applications," *Polymer* 53, no. 23 (2012): 5209–5231, https://doi.org/10.1016/j.polymer.2012.08.053.

49. A. Scotti, M. F. Schulte, C. G. Lopez, J. J. Crassous, S. Bochenek, and W. Richtering, "How Softness Matters in Soft Nanogels and Nanogel Assemblies," *Chemical Reviews* 122, no. 13 (2022): 11675–11700, https://doi.org/10.1021/acs.chemrev.2c00035 From NLM.

50. L. Arleth, X. Xia, R. P. Hjelm, J. Wu, and Z. Hu, "Volume Transition and Internal Structures of Small Poly(N-Isopropylacrylamide) Microgels," *Journal of Polymer Science Part B: Polymer Physics* 43, no. 7 (2005): 849–860, https://doi.org/10.1002/polb.20375.

51. A. Sharma, K. Raghunathan, H. Solhaug, et al., "Modulating Acrylic Acid Content of Nanogels for Drug Delivery & Biocompatibility Studies," *Journal of Colloid and Interface Science* 607 (2022): 76–88, https://doi.org/10.1016/j.jcis.2021.07.139.

52. A. Kardos, T. Gilányi, and I. Varga, "How Small Can Poly(N-Isopropylacrylamide) Nanogels Be Prepared by Controlling the Size With Surfactant?," *Journal of Colloid and Interface Science* 557 (2019): 793–806, https://doi.org/10.1016/j.jcis.2019.09.053.

53. D. Winning, J. K. Wychowaniec, B. Wu, A. Heise, B. J. Rodriguez, and D. F. Brougham, "Thermoresponsiveness Across the Physiologically Accessible Range: Effect of Surfactant, Cross-Linker, and Initiator Content on Size, Structure, and Transition Temperature of Poly(N-Isopropylmethacrylamide) Microgels," *ACS Omega* 9, no. 34 (2024): 36185–36197, https://doi.org/10.1021/acsomega.4c02115.

54. M. Karg, A. Pich, T. Hellweg, et al., "Nanogels and Microgels: From Model Colloids to Applications, Recent Developments, and Future Trends," *Langmuir* 35, no. 19 (2019): 6231–6255, https://doi.org/10.1021/acs.langmuir.8b04304.

55. N. A. Peppas, P. Bures, W. Leobandung, and H. Ichikawa, "Hydrogels in Pharmaceutical Formulations," *European Journal of Pharmaceutics and Biopharmaceutics* 50, no. 1 (2000): 27–46, https://doi.org/10.1016/S0939-6411(00)00090-4.

56. M. Karg, S. Prévost, A. Brandt, D. Wallacher, R. von Klitzing, and T. Hellweg, "Poly-NIPAM Microgels With Different Cross-Linker Densities," in *Intelligent Hydrogels*, ed. G. Sadowski and W. Richtering (Cham, Springer International Publishing, 2013), 63–76.

57. M. K. Yoo, Y. K. Sung, Y. M. Lee, and C. S. Cho, "Effect of Polyelectrolyte on the Lower Critical Solution Temperature of Poly(N-Isopropyl Acrylamide) in the Poly(NIPAAm-Co-Acrylic Acid) Hydrogel," *Polymer* 41, no. 15 (2000): 5713–5719, https://doi.org/10.1016/S0032-3861(99)00779-X.

58. H. Nur, V. T. Pinkrah, J. C. Mitchell, L. S. Benée, and M. J. Snowden, "Synthesis and Properties of Polyelectrolyte Microgel Particles," *Advances in Colloid and Interface Science* 158, no. 1 (2010): 15–20, https://doi.org/10.1016/j.cis.2009.07.008.

59. M. C. Koetting, J. T. Peters, S. D. Steichen, and N. A. Peppas, "Stimulus-Responsive Hydrogels: Theory, Modern Advances, and Applications," *Materials Science & Engineering R: Reports* 93 (2015): 1–49, https://doi.org/10.1016/j.mser.2015.04.001 From NLM.

60. V. Nigro, R. Angelini, M. Bertoldo, E. Buratti, S. Franco, and B. Ruzicka, "Chemical-Physical Behaviour of Microgels Made of Interpenetrating Polymer Networks of PNIPAM and Poly(Acrylic Acid)," *Polymers* 13, no. 9 (2021): 1353.

61. A. D. Drozdov and J. de Claville Christiansen, "Modulation of the Volume Phase Transition Temperature for Multi-Stimuli-Responsive Copolymer Hydrogels," *International Journal of Mechanical Sciences* 211 (2021): 106753, https://doi.org/10.1016/j.ijmecsci.2021.106753.

62. C. G. Lee and T.-H. Kwon, "Controlling Morphologies of Redox-Responsive Polymeric Nanocarriers for a Smart Drug Delivery System," *Chemistry – A European Journal* 29, no. 34 (2023): e202300594, https://doi.org/10.1002/chem.202300594.

63. S. A. Elkassih, P. Kos, H. Xiong, and D. J. Siegwart, "Degradable Redox-Responsive Disulfide-Based Nanogel Drug Carriers via Dithiol Oxidation Polymerization," *Biomaterials Science* 7, no. 2 (2019): 607–617, https://doi.org/10.1039/c8bm01120f.

64. W. Zhou, Y. Jia, Y. Liu, Y. Chen, and P. Zhao, "Tumor Microenvironment-Based Stimuli-Responsive Nanoparticles for Controlled Release of Drugs in Cancer Therapy," *Pharmaceutics* 14, no. 11 (2022): 2346, https://doi.org/10.3390/pharmaceutics14112346.

65. D. Klinger and K. Landfester, "Photo-Sensitive PMMA Microgels: Light-Triggered Swelling and Degradation," *Soft Matter* 7, no. 4 (2011): 1426–1440, https://doi.org/10.1039/C0SM00638F.

66. R. Zhang, T. Liu, W. Li, et al., "Tumor Microenvironment-Responsive BSA Nanocarriers for Combined Chemo/Chemodynamic Cancer Therapy," *Journal of Nanobiotechnology* 20, no. 1 (2022): 223, https://doi.org/10.1186/s12951-022-01442-5.

67. T. Bewersdorff, A. Gruber, M. Eravci, M. Dumbani, D. Klinger, and A. Haase, "Amphiphilic Nanogels: Influence of Surface Hydrophobicity on Protein Corona, Biocompatibility and Cellular Uptake," *International Journal of Nanomedicine* 14 (2019): 7861–7878, https://doi.org/10.2147/ijn.S215935.

68. P. Agnihotri, Sangeeta, S. Aery, and A. Dan, "Temperature- and pH-Responsive Poly(N-Isopropylacrylamide-Co-Methacrylic Acid) Microgels as a Carrier for Controlled Protein Adsorption and Release," *Soft Matter* 17, no. 42 (2021): 9595–9606, https://doi.org/10.1039/D1SM01197A.

69. A. M. Breul, M. D. Hager, and U. S. Schubert, "Fluorescent Monomers as Building Blocks for Dye Labeled Polymers: Synthesis and Application in Energy Conversion, Biolabeling and Sensors," *Chemical Society Reviews* 42, no. 12 (2013): 5366–5407, https://doi.org/10.1039/C3CS35478D.

70. D. Işık, A. A. Joshi, X. Guo, et al., "Sulfoxide-Functionalized Nanogels Inspired by the Skin Penetration Properties of DMSO," *Biomaterials Science* 9, no. 3 (2021): 712–725, https://doi.org/10.1039/D0BM01717E.

71. J. Chen, M. Wu, H. Veroniaina, et al., "Poly(N-Isopropylacrylamide) Derived Nanogels Demonstrated Thermosensitive Self-Assembly and GSH-Triggered Drug Release for Efficient Tumor Therapy," *Polymer Chemistry* 10, no. 29 (2019): 4031–4041, https://doi.org/10.1039/C9PY00537D.

72. M. L. Soriano Pérez, J. A. Funes, C. Flores Bracamonte, et al., "Development and Biological Evaluation of pNIPAM-Based Nanogels as Vaccine Carriers," *International Journal of Pharmaceutics* 630 (2023): 122435, https://doi.org/10.1016/j.ijpharm.2022.122435.

73. M. J. Simpson, B. Corbett, A. Arezina, and T. Hoare, "Narrowly Dispersed, Degradable, and Scalable Poly(Oligoethylene Glycol Methacrylate)-Based Nanogels via Thermal Self-Assembly," *Industrial & Engineering Chemistry Research* 57, no. 22 (2018): 7495–7506, https://doi.org/10.1021/acs.iecr.8b00793.

74. Y. Tian, S. Bian, and W. Yang, "A Redox-Labile Poly(Oligo(Ethylene Glycol)methacrylate)-Based Nanogel With Tunable Thermosensitivity for Drug Delivery," *Polymer Chemistry* 7, no. 10 (2016): 1913–1921, https://doi.org/10.1039/C6PY00057F.

75. F. Xu, J. Zhu, L. Lin, et al., "Multifunctional PVCL Nanogels With Redox-Responsiveness Enable Enhanced MR Imaging and

Ultrasound-Promoted Tumor Chemotherapy," *Theranostics* 10, no. 10 (2020): 4349–4358, https://doi.org/10.7150/thno.43402.

76. K. M. Rao, M. Suneetha, D. V. Kumar, H. J. Kim, Y. J. Seok, and S. S. Han, "Dual Responsive Poly(Vinyl Caprolactam)-Based Nanogels for Tunable Intracellular Doxorubicin Delivery in Cancer Cells," *Pharmaceutics* 14, no. 4 (2022): 852.

Supporting Information

Additional supporting information can be found online in the Supporting Information section.